Molecular Therapy
Nucleic Acids
Original Article

A Functionalized Polydopamine Theranostic Nanoprobe for Efficient Imaging of miRNA-21 and *In Vivo* Synergetic Cancer Therapy

Wenjie Mao,[1,2] Chong Hu,[1,2] Haifeng Zheng,[1] Jinrong Xie,[1] Xiaorui Shi,[1] Yarong Du,[1] and Fu Wang[1]

[1]Engineering Research Center of Molecular and Neuro Imaging, Ministry of Education, School of Life Science and Technology, Xidian University, Xi'an, Shaanxi 710071, China

MicroRNAs (miRNAs) are emerging as vital biomarkers since their abnormal expression is associated with various disease types including cancer. Therefore, it is essential to develop a sensitive and specific platform to monitor the dynamic expression of miRNAs for early clinical diagnosis and treatment. In this study, we designed a functionalized polydopamine (PDA)-based theranostic nanoprobe for efficient detection of miRNA-21 and *in vivo* synergistic cancer therapy. PDA was modified with polyethylene glycol (PEG) and the obtained PDA-PEG nanoparticles showed good stability in different solutions. PDA-PEG nanoparticles were loaded with fluorescein isothiocyanate (FITC)-labeled hairpin DNA (hpDNA) and an anticancer drug doxorubicin (DOX). In the absence of miRNA-21, PDA effectively quenched the fluorescence of FITC-labeled hpDNA. The presence of miRNA-21 specifically recognized hpDNA and induced the dissociation of hpDNA from PDA-PEG and subsequently recovered the fluorescence signals. Upon cellular uptake of these nanoprobes, a dose-dependent fluorescence activation and synergetic cytotoxic effect were observed due to the release of DOX and inhibition of miRNA-21 function. Furthermore, PDA-PEG-DOX-hpDNA nanoparticles can afford long-term monitoring of miRNA-21 and combined therapeutic efficacy in the nude mice bearing 4T1 tumors. Our results demonstrate the capability of PDA-PEG-DOX-hpDNA as a theranostic nanoprobe for continuously tracking of miRNAs and synergetic cancer therapy.

INTRODUCTION

At present, cancer, as one of the main causes of death, is still a huge challenge to global health care.[1–3] Right now, chemotherapy, radiotherapy, and surgery are still the three main cancer treatment methods widely used in the clinic.[4–8] However, these traditional treatment approaches are limited to the low effective absorption of drugs, tumor multidrug resistance, and serious side effects on normal tissues.[9–13] In the past few decades, nanomedicine, which employs nanoparticles as a versatile platform to load imaging agents with different types of therapeutic molecules, has realized image-guided joint cancer therapy with the optimized therapeutic effect.

In recent years, polydopamine (PDA) nanoparticles have been extensively studied due to their good surface modification ability and biocompatibility.[14–17] In addition, another prominent feature of PDA is that its chemical structure contains many functional groups, such as amine, catechol, or imine.[18–21] These functional groups can be used as carriers to covalently modify with the required target nucleic acid molecules or anticancer drugs, which will provide great potential for achieving the combination of chemotherapy and gene therapy in one nanoparticle system due to its strong biocompatibility.[22–25] However, the use of PDA nanoparticles as nanocarrier for co-loading chemotherapy drug and hairpin DNA strands (hpDNAs) to realize the combination of endogenous microRNA (miRNA or miR) detection and cancer therapy has been less studied to our best knowledge.

miRNA is a class of conserved non-coding RNAs, typically 21–23 nucleotides in length.[26] They play an important role in controlling target gene expression by inducing mRNA degradation or suppressing protein translation in a sequence-specific manner, thus providing a post-transcriptional level of gene regulation.[27,28] Among the various miRNAs, miR-21 is significantly upregulated in a variety of tumors, including breast cancer, lung cancer, and liver cancer, suggesting that it may serve as an vital biomarker in tumor progression.[29,30] Therefore, the development of a theranostic platform for tracking intracellular miRNA expression and modulating its function is critical to the miRNA-based cancer diagnosis and therapy.

In this study, we designed a PDA-based nanoprobe as a multifunctional nanocarrier for detecting miRNAs with enhanced therapeutic efficacy (Figure 1). PDA nanoparticles were synthesized using dopamine hydrochloride and functionalized with polyethylene glycol (PEG) to improve their biocompatibility. Such PDA-PEG nanoparticles (PDA-PEG NPs) are suitable for subsequent conjugating fluorescent labeled

Received 4 March 2020; accepted 7 August 2020;
https://doi.org/10.1016/j.omtn.2020.08.007.

[2]These authors contributed equally to this work.

Correspondence: Fu Wang, Engineering Research Center of Molecular and Neuro Imaging, Ministry of Education, School of Life Science and Technology, Xidian University, Xi'an, Shaanxi 710071, China.
E-mail: fwang@xidian.edu.cn

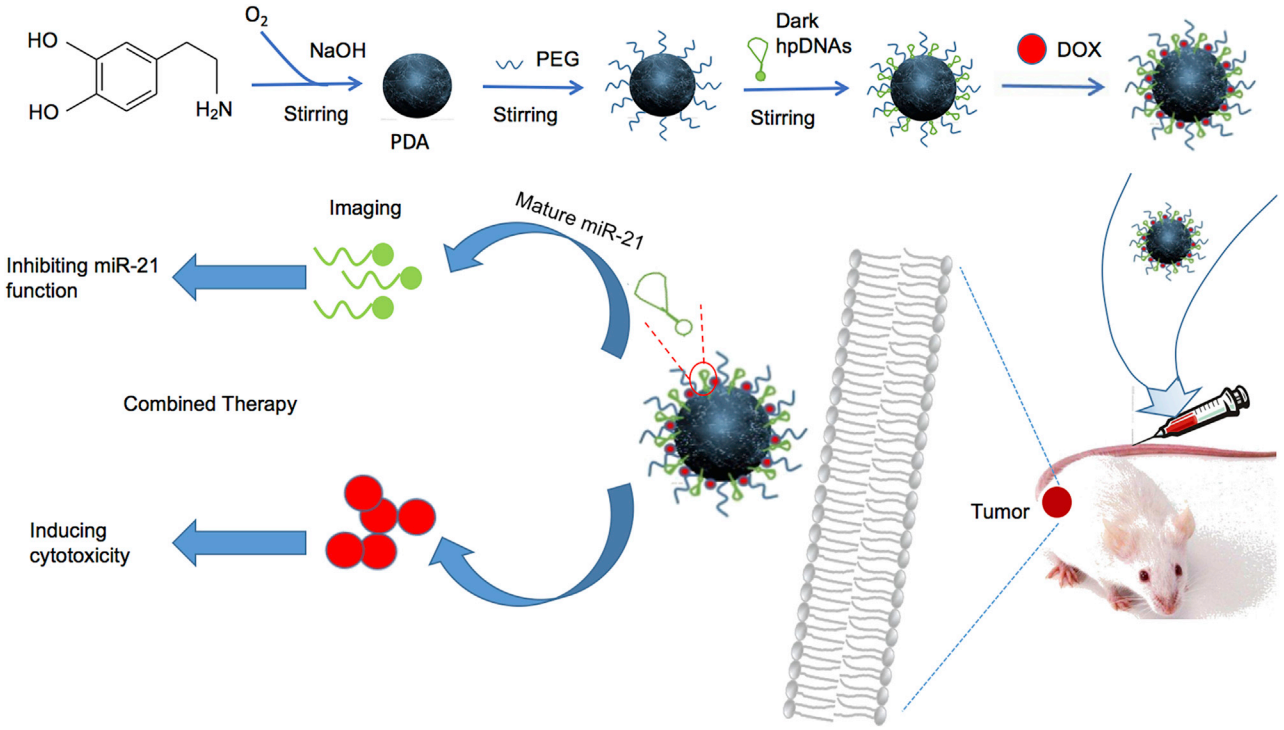

Figure 1. Schematic Illustration of the Development of PEG-PDA Nanoparticles with Coloading Dox and FITC-Labeled hpDNA for Imaging of miRNA-21 and *In Vivo* Synergistic Cancer Treatment

hpDNAs on the surface of PDA by π−π interactions and hydrogen bonding owing to its abundant catechol and amino groups. Meanwhile, a chemotherapeutic drug doxorubicin (DOX) can be also loaded on PDA-PEG NPs with high efficiency to generate a theranostic probe for chemotherapy. In the absence of miR-21, due to the close distance between PDA NPs and hpDNAs and the excellent fluorescence quenching effect of PDA, the immobilized hpDNAs maintain fluorescence quenching state and have no obvious fluorescence on the nanoprobe. In contrast, in the presence of miR-21, miR-21 hybridized with the complementary sequences of hpDNAs, which led to the opening of hpDNAs and weakened the interaction between hpDNA and PDA-PEG NPs, causing the dissociation of immobilized hpDNAs from PDA-PEG NPs and thereafter activating the fluorescence signal of the nanoprobe. Furthermore, hybridization of miR-21 to PDA-PEG-DOX-hpDNA results in a loss of miR-21 function that downregulates tumor suppressor genes such as PTEN or PDCD4. Moreover, the anticancer drug DOX, which is loading in the PDA-PEG NPs, is released inside cells and induces cytotoxicity. Using this nanoprobe, we achieved the efficient detection of miR-21 dynamic expression, as well as combined cancer therapy by inhibiting miR-21 function and triggering cytotoxicity.

RESULTS AND DISCUSSION

Synthesis and Characterization of PDA-PEG-DOX Nanoparticles

PDA was synthesized from dopamine hydrochloride according to our previous protocol.[31] Transmission electron microscopy (TEM) showed that PDA nanoparticles presented uniform spherical morphology (Figure 2A), while the average diameter was around 200 nm as revealed by dynamic light scattering (DLS; Figure 2B). In order to improve the biocompatibility of PDA nanoparticles, we functionalized PDA with amino PEG at pH 10.0, and the obtained PDA-PEG NPs showed excellent biocompatibility in different physiological solutions (Figure 2C). Due to PEG coating, the particle size of PDA-PEG NPs became a little larger compared to PDA (Figure 2B). However, the spectrum absorption characteristics from ultraviolet to near infrared in PDA-PEG solution is similar to that in PDA (Figure 2D).

To test the ability of PDA-PEG to load therapeutic agent, we loaded chemotherapy drug DOX on the surface of PDA-PEG via hydrophobic interaction and π-π stacking. As shown in Figure 3A, the hydrodynamic size of PDA-PEG NPs increased after drug loading, indicating that DOX was successfully loaded on the surface of PDA-PEG to form the PDA-PEG-DOX nanocomposites. Moreover, the zeta potential increased from −34.4 mV to −17.5 mV (Figure S1A). The characteristic absorption peaks appeared in PDA-PEG-DOX solution at 480 nm (Figure S1B), which all proved the successful loading of DOX. In order to explore the drug loading efficiency, the PDA-PEG solution was mixed with different dose of DOX at pH 8.0. The loading ratio of DOX on PDA-PEG NPs was calculated by their UV-vis-NIR spectrum. As shown in Figure 3B, a new absorption peak of 480 nm was found on the PDA-PEG adsorption spectrum

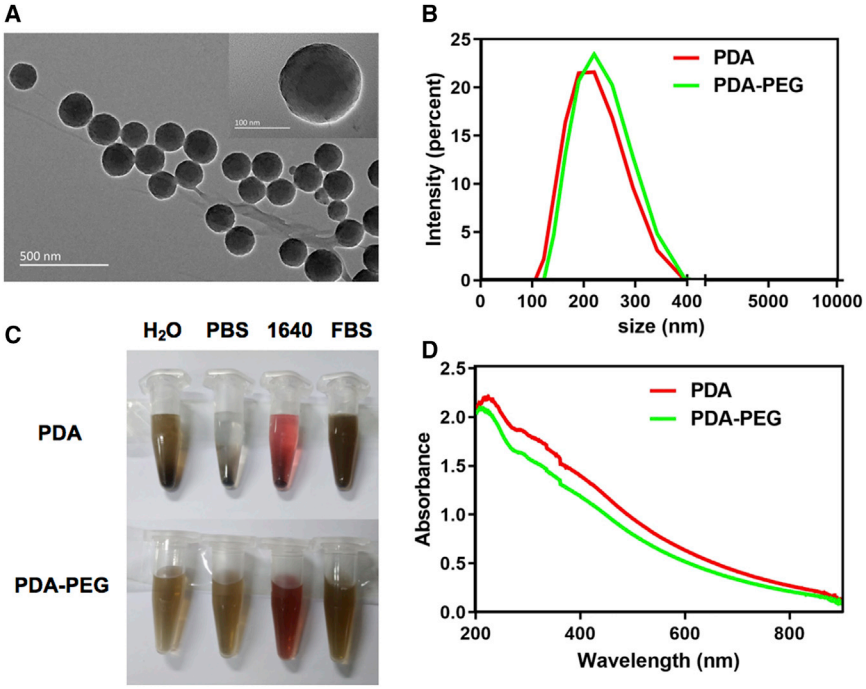

Figure 2. Preparation and Characterization of PDA Nanoparticles

(A) Transmission electron microscope (TEM) images of PDA nanoparticles. Inset shows a magnified image of a single PDA nanoparticle. (B) Size distributions of PDA and PDA-PEG measured with dynamic light scattering (DLS). (C) Photographs of PDA and PDA-PEG dissolved in different solutions (H_2O, PBS, 1640 medium, and FBS). (D) UV-vis-NIR spectra measurement of PDA nanoparticles before and after PEGylation.

after DOX loading, further indicating that DOX was successfully loaded. DOX loading ratio (DOX:PDA-PEG, w/w) increased with the increase of DOX amounts (Figure 3C). When the weight ratio of DOX:PDA-PEG was 2:1, the DOX loading ratio was up to 120%. So PDA-PEG-DOX with DOX:PDA weight ratio of 2:1 was selected for our further experiments.

To examine the drug release behavior of PDA-PEG-DOX, we measured the ultraviolet absorption value of the drug at different pH (5.7 or 7.4). As shown in Figure 3D, the drug release of PDA-PEG-DOX was accelerated at a lower pH. When pH was 5.7, DOX release efficiency could reach 55% at 72 h. When pH was 7.4, DOX release efficiency was less than 15%. This may be due to the protonation of the amino group in the DOX molecule, which makes DOX positively charged and thus enhances hydrophilicity to induce DOX release.

Preparation and Characterization of PDA-PEG-DOX-hpDNA Nanoparticles

To detect miRNAs in living cells, we synthesized a PDA-PEG-DOX-hpDNA nano-drug delivery system. PDA-PEG NPs were used as the quenching agent to quench the fluorescence of hpDNA/fluorescein isothiocyanate (FITC), which specifically recognize miR-21. When endogenous miR-21 is present, FITC-labeled hpDNAs bind to miR-21 and detach from PDA-PEG to generate fluorescence. First, we examined the quenching efficiency of PDA-PEG on DOX. As shown in Figure 4A, DOX exhibited a maximum fluorescence peak at 600 nm. The addition of PDA-PEG reduced the fluorescence intensity of DOX, which was the result of loading DOX onto PDA-PEG NPs. Increasing the concentration of PDA-PEG with DOX at a fixed concentration (50 μg/mL) led to the gradual decrease of fluorescence intensity, indicating that DOX was successfully loaded onto PDA-PEG to form PDA-PEG-DOX nanoparticles. To evaluate quenching efficiency of PDA-PEG on hpDNA, we incubated different concentrations (0, 10, 20, 30, 40, 100, 200 μg/mL) of PDA-PEG NPs with fixed hpDNAs. The FITC fluorescence intensity of hpDNAs decreased with the increased dose of PDA-PEG (Figure 4B; Figure S2A). When the concentration of quenching agent was 24 μg/mL, more than 83% of fluorescence signal was quenched. Similarly, PDA-PEG-DOX nanoparticles also exhibited the effective fluorescence quenching efficiency when incubated with hpDNAs (Figure S2B). To validate the universality of PDA-PEG as quenching agent, we loaded Cy5-labeled hpDNA that specifically target miR-21 on PDA-PEG. We observed that PDA-PEG can efficiently quench more than 70% of Cy5 fluorescence, indicating that the quenching ability of PDA-PEG is independent of the fluorescent dye labeled (Figure 4C).

The PDA-PEG-hpDNA/FITC NPs was then tested for its ability to detect exogenous miR-21 *in vitro*. Although PDA-PEG-hpDNA was quenched in the absence of target miRNAs, the fluorescence recovered in the presence of perfectly complementary targeted miRNAs. With the increased concentration of miR-21 from 1 nM to 50 nM, the fluorescence intensity of PDA-PEG-hpDNA increased in a dose-dependent manner (Figure 4D). In contrast, no significant fluorescence recovery of PDA-PEG-hpDNA was detected in the presence of negative control miR-124a, confirming the binding specificity of miR-21 to PDA-PEG-hpDNA. We then evaluated the stability of the PDA-PEG-hpDNA by incubation in PBS buffer, Opti-MEM medium, and FBS solution for 4 days. During incubation, fluorescence recovery of PDA-PEG-hpDNA occurred only in the presence of exogenous miR-21 (Figure S3).

The Specificity of miR-21 Recognition by PDA-PEG-hpDNA in Cells

To evaluate the theranostic potential of PDA-PEG-hpDNA in cancer cells, we selected 4T1, A549, P19, and 7901 cell lines with high miR-21 expression and MCF-10a, 293, and C2C12 cell lines with low miR-21 expression. PDA-PEG-hpDNA nanoparticles were introduced into

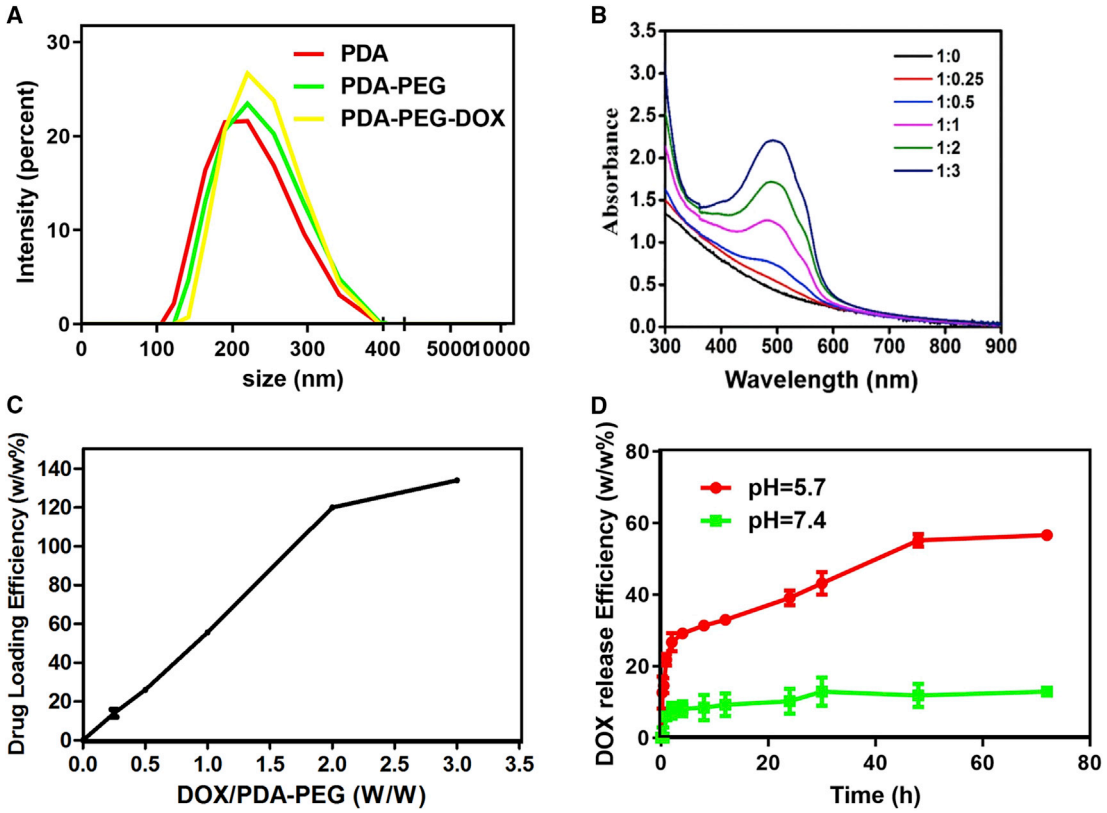

Figure 3. DOX Loading on PDA-PEG

(A) Size distributions of PDA, PDA-PEG, and PDA-PEG-DOX measured with DLS. (B) UV-vis-NIR absorbance spectra of PDA-PEG and PDA-PEG-DOX obtained at different PDA:DOX feeding ratios. (C) Quantification of DOX loading at different feeding amounts of DOX. (D) The drug release from PDA-PEG-DOX in PBS under different pH values.

MCF-10a, 293, and C2C12 cells. In the absence of exogenous miR-21, PDA-PEG-hpDNA was still in the quenching state. As shown in Figure S4, all these three normal cells did not restore the fluorescence of nanoprobe effectively, suggesting that the low expression level of endogenous miR-21 could not bind to the hpDNAs and trigger the dissociation of hpDNAs from PDA NPs. In contrast, in the presence of exogenous miR-21 mimics, the fluorescence intensity was gradually enhanced as the concentration of exogenous miR-21 increased in MCF-10a cells (Figure 5A). miR-124a, which is expressed only during neurogenesis, did not lead to the fluorescence recovery. To detect endogenous miR-21 expression in 4T1 cells, we incubated different concentrations of PDA-PEG-hpDNA nanoparticles with 4T1 cells where miR-21 was highly expressed. With the concentration of PDA-PEG-hpDNA increased, FITC fluorescence intensity increased in a dose-dependent manner (Figure 5B). In contrast, PDA-PEG-hpDNA-Ctrl nanoparticles, which immobilized FITC-labeled control hpDNA with random sequences, did not result in significant increase of fluorescence intensity. In addition, we observed the similar increase trend of fluorescence in P19, A549, and 7901 cells after introduction with PDA-PEG-hpDNA nanoparticles (Figure 5C). Confocal microscopy was performed to further evaluate the fluorescence recovery of PDA-PEG-hpDNA nanoprobe in the present of endogenous miR-21 in 4T1 cells (Figure 5D). It was found that the cytoplasm exhibited green FITC fluorescence and the nucleus presented blue 4′,6-diamidino-2-phenylindole (DAPI) fluorescence, suggesting the effective uptake of PDA-PEG-hpDNA/FITC nanoparticles by the cells and the effective restore of fluorescence activity. However, the control nanoprobe PDA-PEG-hpDNA-ctrl did not exhibit any FITC signal. Taken together, these results confirmed the high specificity of miR-21 recognition by PDA-PEG-hpDNA.

In Vitro Synergistic Therapy in Cells with PDA-PEG-DOX-hpDNA NPs

In view of the excellent performance of PDA-PEG-hpDNA in intracellular uptake, we next want to study the potential toxicity of PDA-PEG-hpDNA in various cancer cells. As shown in Figure 6A, PDA-PEG NPs exhibited no significant toxicity in 4T1 cells even at high concentrations (500 mg mL^{-1}), indicating good biocompatibility of PDA-PEG. The similar results were also observed in P19, A549, and 7901 cells after treatment with PDA-PEG NPs (Figure S5). PDA-PEG-hpDNA induced a slight cytotoxicity in 4T1 cells, which may be owing to the inhibition of endogenous miR-21 function via hybridization of miR-21 to hpDNA (Figure 6B). 4T1 or 7901 cells were then incubated with different concentrations of free DOX, PDA-PEG-DOX, and PDA-PEG-DOX-hpDNA for 48 h (Figures 6C and 6D). The results showed that free DOX was the most toxic,

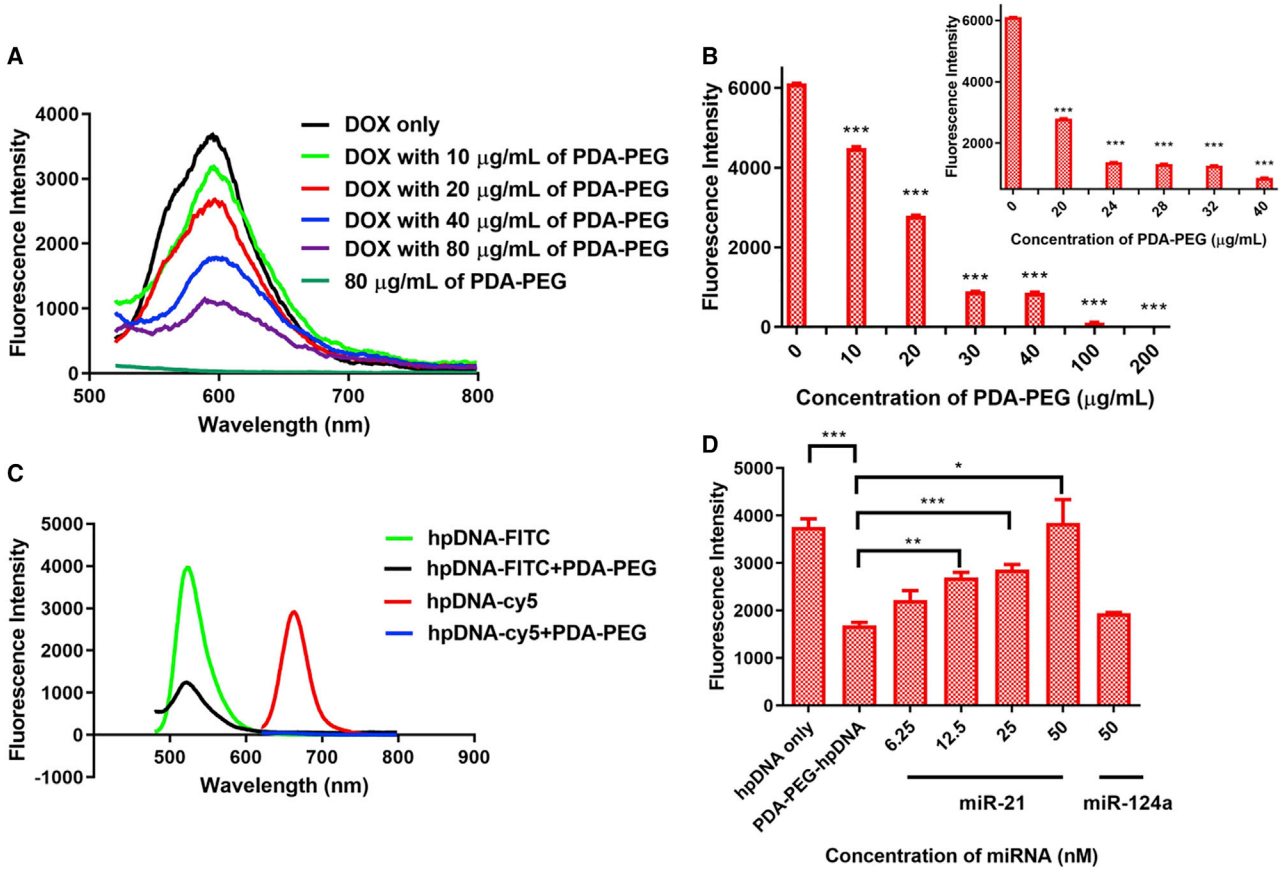

Figure 4. Characterization of PDA-PEG-DOX-hpDNA

(A) Loading of DOX on the surface of PDA-PEG and resultant decrease in the fluorescence intensity of DOX. (B) Quenching efficiency of FITC-hpDNA by PDA-PEG NPs *in vitro*. The FITC fluorescence intensity of hairpin DNA decreased in a quencher concentration-dependent manner. Insert shows that the FITC fluorescence intensity of hairpin DNA decreased in a more detailed quenching concentration gradient. (C) The universality of PDA-PEG nanoparticles for fluorescence quenching. The PDA-PEG NPs can effectively quench Cy5 and FITC fluorescence. (D) Target miR-21 binding specificity of PDA-PEG-hpDNA/FITC NPs *in vitro*. The fluorescence intensity of PDA-PEG-hpDNA/FITC NPs increased in proportion to the concentration of exogenous miR-21. Data are represented as means ± standard deviations of triplicate samples (*$p < 0.05$, **$p < 0.01$, ***$p < 0.001$).

inhibited the cell growth of 4T1 and 7901 cells in a concentration-dependent manner, suggesting no specific toxicity of DOX. PDA-PEG-DOX exhibited weaker toxicity than free DOX did, this may be due to the gradual release of DOX from PDA-PEG-DOX under acidic conditions. We also observed the similar phenomena in P19 and A549 cells (Figure S6). However, the PDA-PEG-DOX-hpDNA nanoprobe presented synergistic inhibition effect compared with single-agent treatment with PDA-PEG-DOX (Figures 6C and 6D). These results suggest that the theranostic nanoprobe based on PDA-PEG-DOX-hpDNA nanocomposite material showed a synergistic effect in killing tumor cells.

In Vivo Imaging of miR-21 and Combined Therapy Using PDA-PEG-DOX-hpDNA

In order to evaluate the performance of the PDA-PEG-DOX-hpDNA nanoprobe for *in vivo* miRNA detection, 4T1 xenografted tumor models were established by subcutaneously injecting 5×10^6 4T1 cells into the right flank of nude mice. PDA-PEG-DOX-hpDNA nanoprobes were injected into mice via tail vein. Fluorescence changes in tumor sites of the nude mice were detected at 0, 1, 3, and 5 days. As shown in Figure 7A, the FITC fluorescence signal in the right buttock of nude mice clearly increased over time, which is due to the high expression of endogenous miR-21 that detached the FITC-hpDNAs from PDA-PEG-DOX-hpDNA NPs through the specific hybridization between NPs and miR-21 in 4T1 cells. The *in vivo* fluorescence activity of PDA-PEG-DOX-hpDNA NPs demonstrated the excellent tumor diagnosis ability of our nanoprobes to monitor the dynamic expression of endogenous miR-21 in a real-time manner.

Due to the great combined therapy efficiency of PDA-PEG-DOX-hpDNA *in vitro*, we next evaluated the *in vivo* performance of our nanoprobe as a theranostic probe to achieve synergistic chemotherapy and gene therapy. The 4T1 xenografted tumor models were randomly divided into 4 groups and received the following different

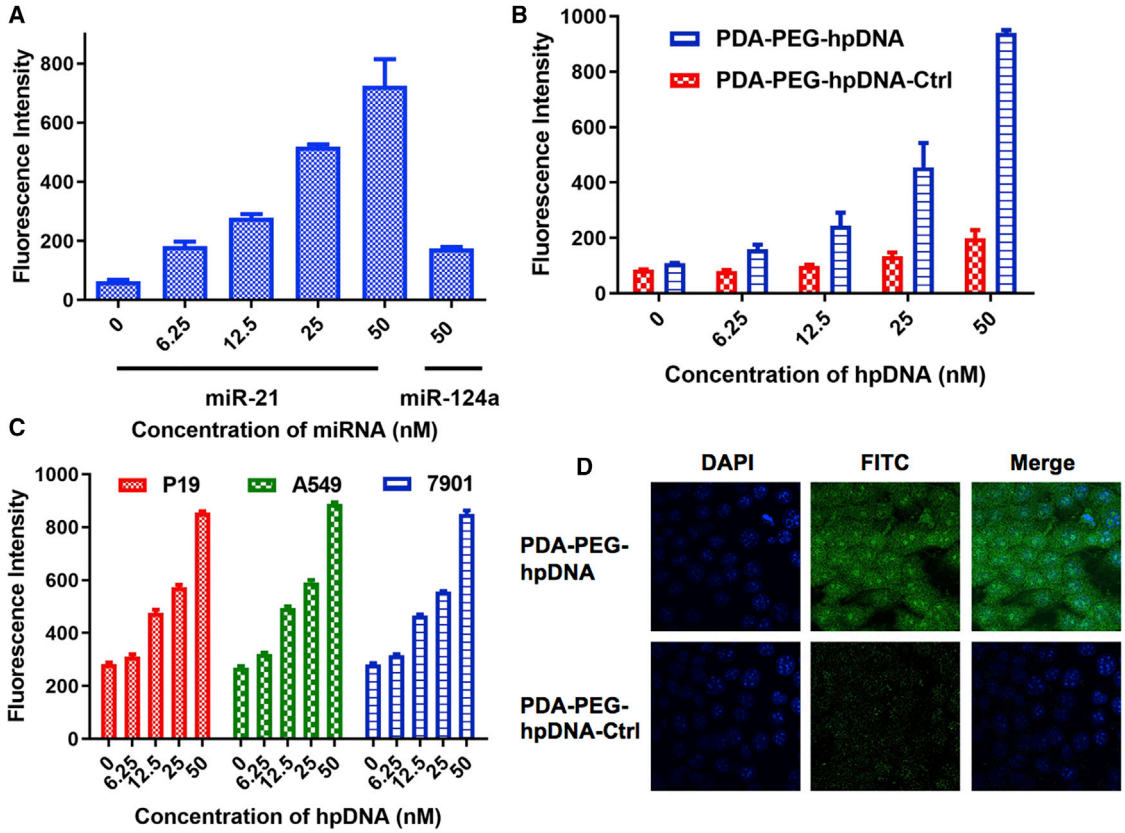

Figure 5. Target miR-21 Specificity of PDA-PEG-DOX-hpDNA NPs in Various Cells

(A) MCF-10A cells transfected with different concentrations of miR-21 mimics were co-incubated with PDA-PEG-hpDNA NPs for 24 h. Then the fluorescence intensity was measured. miR-124a was selected as the negative control. (B) Specificity of PDA-PEG-hpDNA for detection of endogenous miR-21 in 4T1 cells. The endogenous miR-21 in 4T1 cells was specifically hybridized with PDA-PEG-hpDNA and its fluorescence intensity was found to increase in a dose-dependent manner. Target specificity was further confirmed by PDA-PEG-hpDNA-Ctrl with disrupted sequences. Data are represented as means ± standard deviations of triplicate samples. (C) Fluorescence intensity of P19, A549, and 7901 cells co-incubated with different concentrations of PDA-PEG-hpDNA NPs. (D) Confocal microscopy images (×800) of 4T1 cells incubated with different concentrations of PDA-PEG-hpDNA or PDA-PEG-hpDNA-Ctrl. Blue signal indicates DAPI (nucleus: 490 nm) and green signal indicates FITC (excitation/emission: 480/520 nm).

treatment: (1) PBS, (2) PDA-PEG-hpDNA, (3) PDA-PEG-DOX, and (4) PDA-PEG-DOX-hpDNA. As shown in Figure 7B, compared with control mice treated with PBS, the tumor growth rate in mice receiving PDA-PEG-hpDNA treatment was slightly reduced. In contrast, the PDA-PEG-DOX-hpDNA group showed more effective inhibition of tumor growth than PDA-PEG-DOX or PDA-PEG-hpDNA treated mice, indicating the remarkable synergistic effect of PDA-PEG-DOX-hpDNA nanoprobes in combination therapy. The tumor sizes further confirmed the treatment effect of different groups (Figure 7C). However, the body weight of the mice with different treatments was monitored and exhibited no obvious change during the process, indicating that the *in vivo* toxicity were negligible (Figure 7D).

In addition, we further detected the fluorescence signals in the main organs and tumors from different treatment groups using the IVIS imaging system. The results demonstrated that the tumors from PDA-PEG-hpDNA and PDA-PEG-DOX-hpDNA group exhibited obvious fluorescence enhancement, implying the effective delivery of nanoprobes into 4T1 tumors and target recognition of endogenous miR-21 (Figure 8A). Meanwhile, the livers also showed certain fluorescence signals since they were the main metabolic detoxification organs. To further investigate the potential toxicity of PDA-PEG-DOX-hpDNA, we performed hematoxylin and eosin (H&E) staining to analyze the main organs of mice in the different treatment groups. No obvious morphological changes were observed in the main organs (heart, liver, spleen, lung, and kidney) collected from the nanoprobe treatment group, indicating that the nanoparticles had good biological safety (Figure 8B). However, the H&E staining results from tumor sections demonstrated that partial tumor damages were found in mice after treatment with PDA-PEG-DOX or PDA-PEG-DOX-hpDNA (Figure S7). Of note, tumors receiving PDA-PEG-DOX-hpDNA showed the severest morphological damage, further confirming the combined therapeutic efficacy of PDA-PEG-DOX-hpDNA as theranostic agent in cancer treatment. Taken together, these results demonstrate that the PDA-PEG-DOX-hpDNA nanoprobes enables

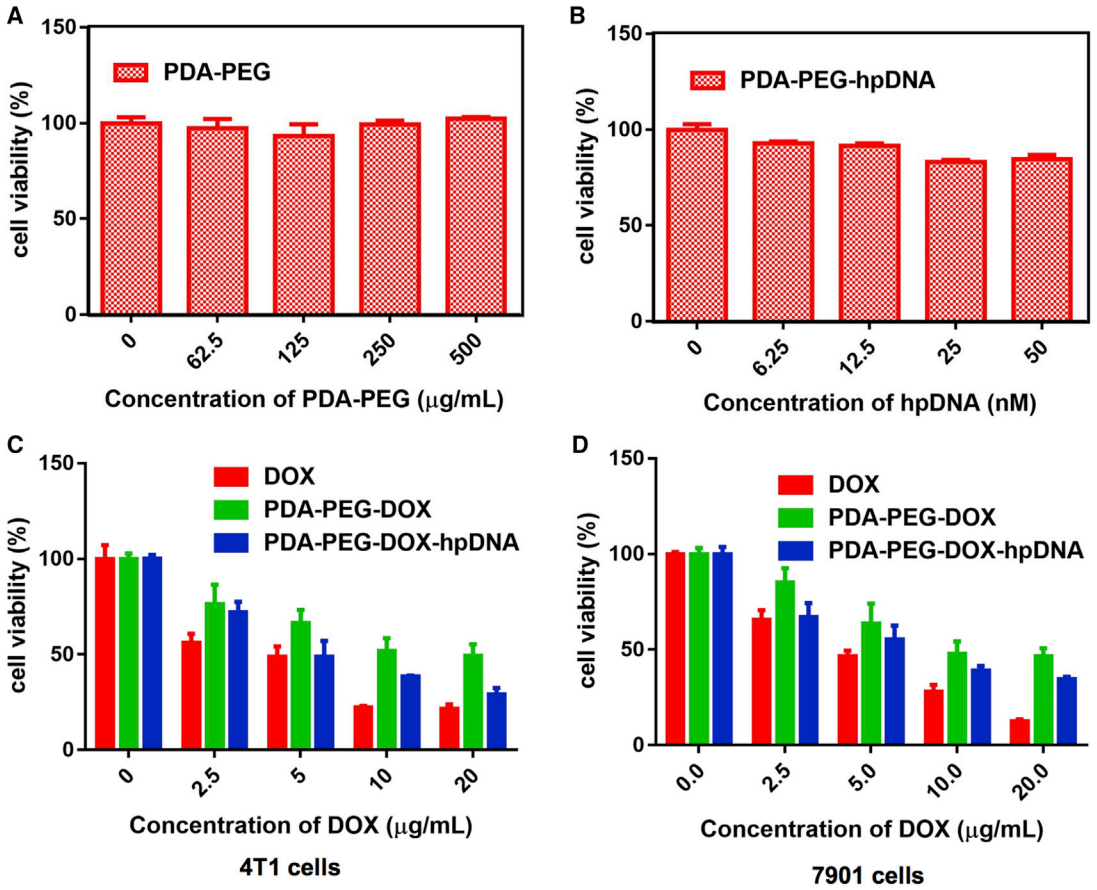

Figure 6. *In Vitro* Cytotoxicity Induced by PDA-PEG-DOX-hpDNA Nanoparticles

(A and B) The cell viabilities of 4T1 cells after being incubated with different concentrations of (A) PDA-PEG or (B) PDA-PEG-hpDNA for 24 h. (C and D) The relative cell viabilities of (C) 4T1 cells or (D) 7901 cells after being incubated with different concentrations of free DOX, PDA-PEG-DOX, or PDA-PEG-DOX-hpDNA (0, 2.5, 5, 10, 20 μg/mL of DOX) for 48 h.

effective imaging of miR-21 and synergistic suppression of tumors *in vivo*.

Conclusions

In summary, our study proposed a PDA-based theranostic nanoprobe for efficient imaging of miRNA-21 and *in vivo* synergetic cancer therapy. In this system, PDAs were prepared from dopamine and modified with PEG under weak alkaline condition. The obtained PDA-PEG NPs have good physiological stability. PDA-PEG was then used as a carrier for chemotherapy drug DOX loading with high loading efficiency. In addition, PDA-PEG was employed as a fluorescence quenching agent to immobilize FITC-labeled hpDNA for targeted imaging of miR-21 in cancer cells. Our results demonstrated that PDA-PEG-DOX-hpDNA not only enabled real-time detect the dynamic expression of specific miRNAs, but also allowed excellent combined cancer therapy in living cells and mice. Considering that there were no significant side effects on the main organs of mice, PDA-PEG-DOX-hpDNA may hold great potential as an effective and safe nanoprobe for monitoring other cancer-related miRNAs with combined treatment and diagnosis of multiple cancers.

MATERIALS AND METHODS

Cell Culture

P19, 7901, A549, MCF-10A, 293, and C2C12 cells were cultured in a standard incubator (5% CO_2 atmosphere at 37°C), supplemented with Dulbecco's modified Eagle's medium (DMEM, Hyclone, USA), 10% fetal bovine serum (FBS, Hyclone, USA), and 1% streptomycin/penicillin solution (Hyclone, USA). 4T1 cells were cultured in 1640 medium (GIBCO, USA) with 10% FBS and 1% antibiotic solution.

Synthesis and Functionalization of PDA Nanoparticles

PDA nanoparticles were synthesized according to our published protocols with a little modification.[31] In brief, 180 mg of dopamine hydrochloride (Aldrich Chemical) was dissolved in 90 mL of deionized water, and then 760 μL of sodium hydroxide (NaOH, 1 mol L^{-1}) was added. After magnetic stirring at 50°C for 5 h, the PDA nanoparticles

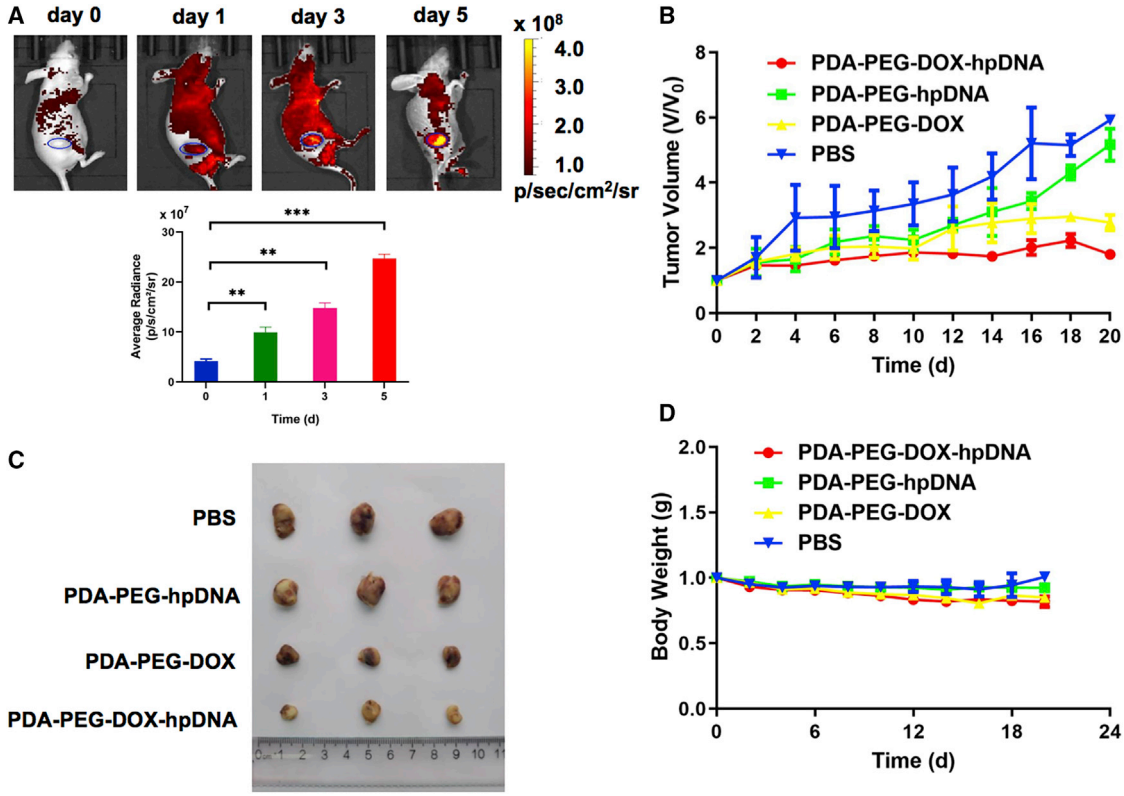

Figure 7. *In Vivo* Combination Therapy and Fluorescence Imaging Based on PDA-PEG-DOX-hpDNA Nanoprobe

(A) Upper shows *in vivo* fluorescence imaging of 4T1 xenografted tumor models after i.v. injection of PDA-PEG-hpDNA at day 0, 1, 3, and 5. The blue circle showed the tumor site. Lower shows the quantification of the fluorescence signals from the region of interest in mice. (B) Tumor growth curves of mice with different treatments given at every 2 days. Each group is as follows: (1) PBS, (2) PDA-PEG-DOX, (3) PDA-PEG-hpDNA, and (4) PDA-PEG-DOX-hpDNA. Doses for each injection: 5 mg kg^{-1} of DOX. The tumor volumes were normalized to their initial sizes. (C) The representative images of tumor tissues treated with the different groups. (D) Average body weights of mice after various treatments indicated in (B).

were collected by centrifugation at 12,000 × *g* and then washed with deionized water until no color remained. The PDA nanoparticles were then covalently modified by amine-terminated PEG (mPEG-NH_2, 5 kDa). 47 mg of mPEG-NH_2 was dissolved in 4 mL of deionized water and then was added into 1 mL of PDA solution (4.667 mg mL^{-1}) at pH 8.0. The reaction solution was stirred overnight. The obtained PDA-PEG NPs were purified by filtration through 10 kDa MWCO Amicon filters to remove excess PEG.

Design of hpDNA/FITC and Synthesis of PDA-PEG-hpDNA/FITC

Mature miR-21 and miR-124a mimics were purchased from Shanghai Generay Biotech. miR-124a was used as a negative control. The sequences of the miRNAs are as follows: miR-21, 5′-UAG CUU AUC AGA CUG AUG UUG A-3′; miR-124a, 5′-UAA GGC ACG CGG UGA AUG CC-3′. A FITC-labeled hpDNA oligo containing miR-21 binding sequence was synthesized. In addition, a control hpDNA that does not contain miR-21 binding sequence was also synthesized. The sequences are as follows: hpDNA-miR21, 5′-FITC-CCG TTC TAT CAA CAT CAG TCT GAT AAG CTA TAG AAC GG-3′; hpDNA-ctrl: 5′-FITC-CCG TTC TAC CAA CCC GCT AGC TCG GG A CTA TAG AAC GG-3′. PDA-PEG-hpDNA nanoparticles were prepared by immobilizing fluorescent labeled hpDNAs on the PDA-PEG NPs surface. Briefly, 500 μL of 100 nM DNA solution was mixed with the dispersible nanoparticles of different concentrations and stirred at room temperature for 1 h. The pellets are redispersed in water to restore the initial concentration of the PDA-PEG NP.

DOX Loading and Release

DOX was purchased from Shanghai Aladdin Bio-Chem Technology. To load DOX onto PDA-PEG, we mixed 1 mL of PDA-PEG solution (1 mg mL^{-1}) with different amounts of DOX (0.25–3 mg) in phosphate buffer at pH 8.0. The mixture was stirred overnight in the dark at room temperature. Then the excess DOX was removed by filtration with 10 kDa MWCO filters. The obtained DOX-loaded PDA-PEG NPs (PDA-PEG-DOX) were re-suspended in deionized water and stored at 4°C. The loading efficiency of DOX was measured by ultraviolet-visible-near infrared spectroscopy (UV-vis-NIR). Fluorescence spectra of free DOX and PDA-PEG-DOX were measured by F7000 Fluorescence Spectrometer. For DOX releasing measurement, PDA-PEG-DOX solutions were dialyzed in PBS at pH 5.7 and 7.4 in 37°C water bath. At different time points, DOX released from PDA-PEG-DOX was collected and measured by UV-vis-NIR spectra.

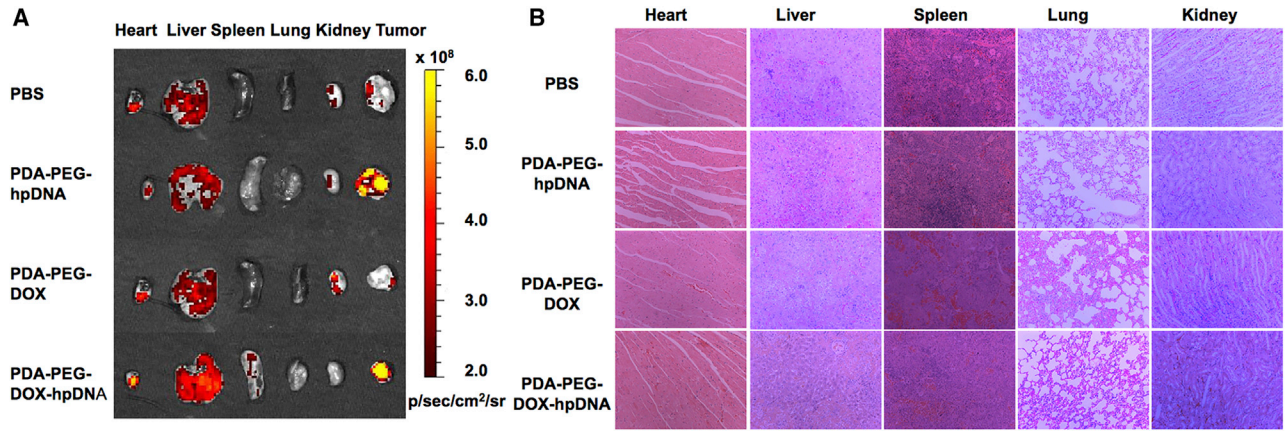

Figure 8. *Ex Vivo* Fluorescence Imaging and H&E Staining of Tissues

(A) Fluorescence imaging of major organs and tumor tissues collected from different treatment groups. (B) The representative images for H&E staining of major organs.

Quenching and Release Assay

To monitor FITC-labeled hpDNAs on the surfaces of PDA-PEG or PDA-PEG-DOX nanoparticles, we used fluorescence spectrophotometer (Hitachi F7000, Hitachi) for fluorescence measurement. In short, FITC hpDNAs and PDA-PEG NPs were incubated at room temperature in dark for 1 h to determine the fluorescence intensity of the mixed solution. Fluorescence signal from free hpDNAs solution was recorded as reference to calculate the quenching efficiency of nanoparticles. Subsequently, the nanoprobe carrying the immobilized FITC-labeled hpDNAs (100 nM) was mixed with miR-21 mimics at different concentrations (0, 6.25, 12.5, 25, 50, 100, 200 nM) or miR-124a (50 nM) as a control. The fluorescence intensity in the mixed solution was measured every day to observe the recovery of nanoparticles and to screen out the optimal target concentration. Subsequently, PBS solution, opti-MEM solution, and fetal bovine serum solution with FITC-labeled hpDNAs (100 nM) were added in day 0, 2, and 4 with the optimal concentration of the target miRNAs to observe the fluorescence change of the nano-probes and evaluate the stability of the nanoprobes. The recorded fluorescence intensity was compared with the reference intensity.

Cell Viability Assay and Optical Measurement

4T1, P19, A549, and 7901 cells were seeded into 96-well plates at a density of 9,000∼12,000 cells per well overnight, and then incubated with different concentrations of free DOX (0, 2.5, 5, 10, and 20 μg/mL), PDA-PEG (0, 62.5, 125, 250, 500 μg/mL), free hpDNA (0, 6.25, 12.5, 25, 50 nM), and PDA-PEG-DOX, PDA-PEG-DOX-hpDNA (0, 2.5, 5, 10, and 20 μg/mL of DOX) for 48 h in a humidified atmosphere containing 5% CO_2 at 37°C. Cell counting kit-8 (CCK-8) assay was then conducted to determine the relative cell viabilities compared to the untreated cells. The optical density was read at 450 nm using a microplate reader (GloMax Discover, Promega, USA).

To evaluate the fluorescence diagnostic potential of nanoprobe, we selected 4T1, P19, A549, and 7901 cells with high expression of miR-21 and MCF-10A, 293, C2C12 cells with low expression of miR-21. All of these cells were pre-cultured in 24-well plates (50,000 per dish) for 24 h, then incubated with different concentration of PDA-PEG-hpDNA (0, 6.25, 12.5, 25, 50 nM). The fluorescence changes caused by intracellular miR-21 were detected by microplate reader (GloMax Discover, Promega, USA) after incubation for 24 h.

To evaluate the targeting specificity of nanoprobe, we selected 4T1 tumor cells and MCF-10A normal cells. After 24 h of pre-cultured, for 4T1 cells, incubated with different concentration of PDA-PEG-hpDNA and PDA-PEG-hpDNA-ctrl (0, 6.25, 12.5, 25, and 50 nM). For MCF-10a cells, PDA-PEG-hpDNA (50 nM) were first added to incubated 24 h, then exogenous miR-21 (0, 6.25, 12.5, 25, and 50 nM) and miR-124a (50 nM) were added, and fluorescence changes were detected by microplate reader (GloMax Discover, Promega, USA) after incubation for 24 h.

In Vitro Confocal Fluorescence

4T1 cells seeded into confocal dish (30,000 per dish) were incubated with PDA-PEG-hpDNA/FITC or PDA-PEG-hpDNA-Ctrl (50 nM of hpDNA) for 24 h. Subsequently, the cells were washed with PBS for three times and stained with DAPI to label cell nucleus and then imaged by a laser scanning confocal fluorescence microscope (Olympus).

Animal Model

The animal studies were conducted with the Guidance for the Care and Use of Laboratory Animals approved by Xidian University. Female BALB/c-nu mice were purchased from Beijing HFK Bioscience. 5×10^6 4T1 cells suspended in 150 μL of PBS solution were subcutaneously injected into the right buttock of each mouse. The mice were used for imaging and treatment when the tumor volume reached $\approx 100\ mm^3$.

In Vivo Imaging and Combined Therapy

For *in vivo* imaging study, when the tumor volume of mice reached 100 mm^3, one group of mice (n = 5) were intravenously (i.v.) received

with PDA-PEG-hpDNA/FITC nanoparticles (4 mg/kg of PDA-PEG per mouse), the other group of mice (n = 5) were injected with PBS and used as control. For imaging experiment, mice were anesthetized with 1.5% isoflurane in O_2 gas at a flow rate of 1 L/min. *In vivo* fluorescence imaging was conducted using a blue filter (Ex: 480 nm, Em: 520 nm). The mice were scanned using the IVIS spectrum imaging system (Caliper Life Sciences, MA, USA).

For combined therapy, mice bearing 4T1 tumor model were randomly divided into four groups (n = 6) for different treatments including: PBS, PDA-PEG-hpDNA, PDA-PEG-DOX (5 mg kg^{-1} of DOX), and PDA-PEG-DOX-hpDNA (5 mg kg^{-1} of DOX). The above agents were i.v. injected into xenograft mice every 2 days. The tumor volume was calculated according to the formula: (width)2 *length/2. The length and width of the tumor diameter were measured by digital caliper every other day.

Statistical Analysis

All data are presented as mean standard deviation unless otherwise stated. Student's t test was used for statistical analysis. p value <0.05 was considered statistically significant.

SUPPLEMENTAL INFORMATION

Supplemental Information can be found online at https://doi.org/10.1016/j.omtn.2020.08.007.

AUTHOR CONTRIBUTIONS

W.M. performed most of the experiments. C.H., H.Z., and J.X. helped to perform the experiments. X.S. and Y.D. helped to analyze the data. W.M. wrote the manuscript draft. F.W. conceived and designed the experiments, analyzed the data, and finalized the manuscript.

CONFLICTS OF INTEREST

The authors declare no competing interests.

ACKNOWLEDGMENTS

This work was supported by National Natural Science Foundation of China (no. 81772010) and The National Key Research and Development Program of China (973 Program; grant number 2017YFA0205202).

REFERENCES

1. Fan, L., Strasser-Weippl, K., Li, J.-J., St. Louis, J., Finkelstein, D.M., Yu, K.-D., Chen, W.-Q., Shao, Z.-M., and Goss, P.E. (2014). Breast cancer in China. The Lancet Oncology *15*, e279–e289.

2. Yoo, D., Lee, J.-H., Shin, T.-H., and Cheon, J. (2011). Theranostic magnetic nanoparticles. Acc. Chem. Res *44*, 863–874.

3. Siegel, R.L., Miller, K.D., and Jemal, A. (2017). Cancer Statistics, 2017. CA Cancer J. Clin. *67*, 7–30.

4. Breugom, A.J., Swets, M., Bosset, J.F., Collette, L., Sainato, A., Cionini, L., Glynne-Jones, R., Counsell, N., Bastiaannet, E., van den Broek, C.B., et al. (2015). Adjuvant chemotherapy after preoperative (chemo)radiotherapy and surgery for patients with rectal cancer: a systematic review and meta-analysis of individual patient data. Lancet Oncol. *16*, 200–207.

5. Buchholz, T.A., Mittendorf, E.A., and Hunt, K.K. (2015). Surgical considerations after neoadjuvant chemotherapy: breast conservation therapy. J. Natl. Cancer Inst. Monogr *2015*, 11–14.

6. Brunner, T.B. (2016). The rationale of combined radiotherapy and chemotherapy - Joint action of Castor and Pollux. Best Pract. Res. Clin. Gastroenterol. *30*, 515–528.

7. Howard, J., Masterson, L., Dwivedi, R.C., Riffat, F., Benson, R., Jefferies, S., Jani, P., Tysome, J.R., and Nutting, C. (2016). Minimally invasive surgery versus radiotherapy/chemoradiotherapy for small-volume primary oropharyngeal carcinoma. Cochrane Database Syst. Rev. *12*, CD010963.

8. Ethun, C.G., Bilen, M.A., Jani, A.B., Maithel, S.K., Ogan, K., and Master, V.A. (2017). Frailty and cancer: Implications for oncology surgery, medical oncology, and radiation oncology. CA Cancer J. Clin. *67*, 362–377.

9. Tian, Y., Jiang, X., Chen, X., Shao, Z., and Yang, W. (2014). Doxorubicin-loaded magnetic silk fibroin nanoparticles for targeted therapy of multidrug-resistant cancer. Adv. Mater *26*, 7393–7398.

10. Min, Y., Mao, C.Q., Chen, S., Ma, G., Wang, J., and Liu, Y. (2012). Combating the drug resistance of cisplatin using a platinum prodrug based delivery system. Angew. Chem. Int. Ed. Engl *51*, 6742–6747.

11. Kirtane, A.R., Kalscheuer, S.M., and Panyam, J. (2013). Exploiting nanotechnology to overcome tumor drug resistance: challenges and opportunities. Adv. Drug Deliv. Rev *65*, 1731–1747.

12. Ma, X.-w., Zhao, Y.-l., and Liang, X.-j. (2011). Nanodiamond delivery circumvents tumor resistance to doxorubicin. Acta. Pharmacol. Sin *32*, 543.

13. Mura, S., Nicolas, J., and Couvreur, P. (2013). Stimuli-responsive nanocarriers for drug delivery. Nat. Mater *12*, 991–1003.

14. Liu, Y., Ai, K., and Lu, L. (2014). Polydopamine and Its Derivative Materials: Synthesis and Promising Applications in Energy, Environmental, and Biomedical Fields. Chem. Rev *114*, 5057–5115.

15. Park, J., Brust, T.F., Lee, H.J., Lee, S.C., Watts, V.J., and Yeo, Y. (2014). Polydopamine-Based Simple and Versatile Surface Modification of Polymeric Nano Drug Carriers. ACS. Nano *8*, 3347–3356.

16. Choi, C.K., Li, J., Wei, K., Xu, Y.J., Ho, L.W., Zhu, M., To, K.K., Choi, C.H., and Bian, L. (2015). A gold@polydopamine core-shell nanoprobe for long-term intracellular detection of microRNAs in differentiating stem cells. J. Am. Chem. Soc. *137*, 7337–7346.

17. Zhang, P., Li, J., Ghazwani, M., Zhao, W., Huang, Y., Zhang, X., Venkataramanan, R., and Li, S. (2015). Effective co-delivery of doxorubicin and dasatinib using a PEG-Fmoc nanocarrier for combination cancer chemotherapy. Biomaterials *67*, 104–114.

18. Ju, K.Y., Lee, Y., Lee, S., Park, S.B., and Lee, J.-K. (2011). Bioinspired Polymerization of Dopamine to Generate Melanin-Like Nanoparticles Having an Excellent Free-Radical-Scavenging Property. Biomacromolecules *12*, 625–632.

19. Qian, L., Wang, N., Caro, J., and Huang, A. (2013). Biol.-Inspired Polydopamine: A Versatile and Powerful Platform for Covalent Synthesis of Molecular Sieve Membranes. J. Am. Chem. Soc *135*, 17679–17682.

20. Yan, J., Yang, L., Lin, M.F., Ma, J., Lu, X., and Lee, P.S. (2013). Polydopamine Spheres as Active Templates for Convenient Synthesis of Various Nanostructures. Small *9*, 596–603.

21. Huang, S., Liang, N., Hu, Y., Zhou, X., and Abidi, N. (2016). Polydopamine-Assisted Surface Modification for Bone Biosubstitutes. Biomed Res. Int *2016*, 2389895.

22. Zhong, X., Yang, K., Dong, Z., Yi, X., Wang, Y., Ge, C., Zhao, Y., and Liu, Z. (2016). Polydopamine as a Biocompatible Multifunctional Nanocarrier for Combined Radioisotope Therapy and Chemotherapy of Cancer. Adv. Funct. Mat *25*, 7327–7336.

23. Dong, Z., Hua, G., Min, G., Zhu, W., Sun, X., Feng, L., Fu, T., Li, Y., and Liu, Z. (2016). Polydopamine Nanoparticles as a Versatile Molecular Loading Platform to Enable Imaging-guided Cancer Combination Therapy. Theranostics *6*, 1031–1042.

24. Tang, W., Liu, B., Wang, S., Liu, T., Fu, C., Ren, X., Tan, L., Duan, W., and Meng, X. (2016). Doxorubicin-loaded ionic liquid–polydopamine nanoparticles for combined chemotherapy and microwave thermal therapy of cancer. RSC Advances *6*, 32434–32440.

25. Zhao, H., Chao, Y., Liu, J., Huang, J., Pan, J., Guo, W., Wu, J., Sheng, M., Yang, K., Wang, J., et al. (2016). Polydopamine Coated Single-Walled Carbon Nanotubes as

a Versatile Platform with Radionuclide Labeling for Multimodal Tumor Imaging and Therapy. Theranostics *6*, 1833–1843.

26. Stefani, G., and Slack, F.J. (2008). Small non-coding RNAs in animal development. Nat. Rev. Mol. Cell Biol *9*, 219–230.

27. Hobert, O.J. (2008). Gene regulation by transcription factors and microRNAs. Science *319*, 1785–1786.

28. Huntzinger, E., and Izaurralde, E. (2011). Gene silencing by microRNAs: contributions of translational repression and mRNA decay. Nature Reviews Genetics *12*, 99–110.

29. Wang, F., Zhang, B., Zhou, L., Shi, Y., Li, Z., Xia, Y., and Tian, J. (2016). Imaging Dendrimer-Grafted Graphene Oxide Mediated Anti-miR-21 Delivery With an Activatable Luciferase Reporter. ACS Appl. Mater. Interfaces *8*, 9014–9021.

30. Liu, W., Zhang, B., Chen, G., Wu, W., Zhou, L., Shi, Y., Zeng, Q., Li, Y., Sun, Y., Deng, X., and Wang, F. (2017). Targeting miR-21 with Sophocarpine Inhibits Tumor Progression and Reverses Epithelial-Mesenchymal Transition in Head and Neck Cancer. Mol. Ther. *25*, 2129–2139.

31. Li, Z., Wang, B., Zheng, Z., Bo, W., Xu, Q., Mao, W., Tian, J., Yang, K., and Wang, F. (2018). Radionuclide imaging-guided chemo-radioisotope synergistic therapy using I-131 labeled polydopamine multifunctional nanocarrier. Mol. Ther *26*, 1385–1983.